Med Ultrason 2026, Vol. 28, no. 2, 241-242

Three-dimensional physical models of fetal hearts with congenital heart diseases

Nathalie Jeanne Bravo-Valenzuela[1], Maria de Fátima Monteiro Pereira Leite[2,3], Edward Araujo Júnior[4,5], Gerson Ribeiro[2], Caroline Oliveira Nieblas[5], Heron Werner[2]

[1]Department of Pediatrics, Pediatric Cardiology, School of Medicine, Federal University of Rio de Janeiro (UFRJ), Rio de Janeiro, [2]Department of Fetal Medicine, Biodesign Laboratory DASA / PUC, Rio de Janeiro, [3]Fetal Cardiology Sector, Fernandes Figueira Institute (IFF / FIOCRUZ), Rio de Janeiro, [4]Department of Obstetrics, Paulista School of Medicine, Federal University of São Paulo (EPM-UNIFESP), São Paulo, [5]Discipline of Woman Health, Municipal University of São Caetano do Sul (USCS), São Caetano do Sul, Brazil

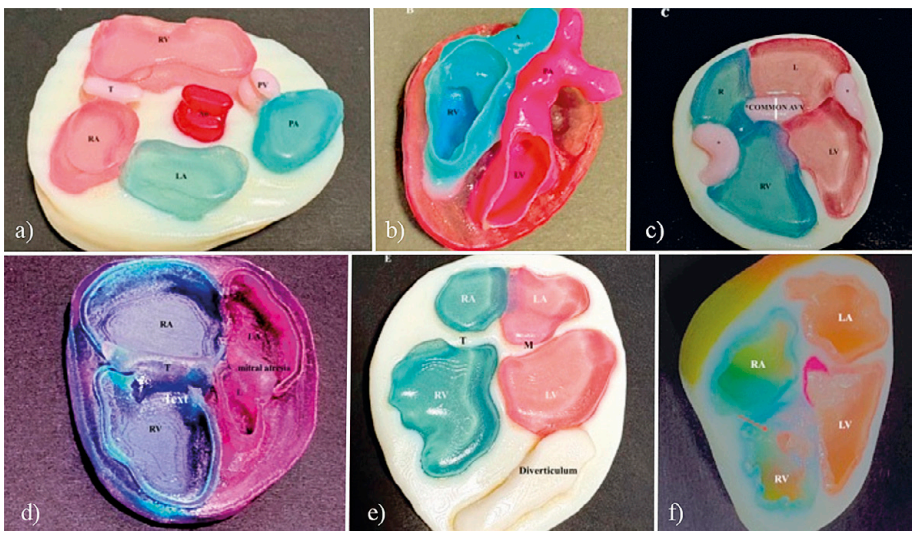


Fig 1. 3D physical models: a) Double Outlet of Right Ventricle; b) Transposition of Great Arteries; c) Hypoplastic Left Heart Syndrome; d) Complete form of Atrioventricular Septal Defect; e) Ventricular Septal Defect; and f) Left Ventricle Diverticulum. LV: left ventricle; RV: right ventricle; LA: left atrium; RA: right atrium; Ao; aorta; PA: pulmonary artery; VSD: ventricular septal defect; *common AV valve: common atrioventricular valve.

To the Editor,

Congenital heart disease (CHD) is the most prevalent birth defect ranging from 4/1,000 to 50/1,000, being an important cause of perinatal mortality [1]. Three-dimensional (3D) ultrasound of the fetal heart with Spatio-Temporal Image Acquisition (STIC) has engendered anatomical detailing and enhanced the accuracy of prenatal diagnosis [2]. Subsequent advancements in 3D reconstruction software, in conjunction with high-resolution 3D printers, have enabled the optimization of 3D-printed models [3,4].

The advent of 3D printing represents a significant advance in this field, offering a promising method for the prenatal diagnosis of CHD. This pioneering technology has the potential to provide detailed anatomical information that improves diagnostic accuracy, supports multidisciplinary understanding, enhances mother–fetus interaction in blind pregnant women, and enables remote team collaboration (shortening long distances) [5].

Received 23.03.2026 Accepted 18.05.2026
Med Ultrason
2026, Vol. 28, No 2, 241-242, DOI: 10.11152/mu-4620,
Corresponding author: Prof. Edward Araujo Júnior, PhD
Rua Belchior de Azevedo,
156 apto. 111 Torre Vitoria
São Paulo – SP, Brazil
CEP 05089-030
E-mail: araujojred@terra.com.br

Some groups have reported 3D-printed fetal models of CHDs, however there is a paucity of literature regarding its applicability in prenatal counselling and birth planning for CHD [6,7]. In this scenario, 16 3D physical models of fetal hearts were reconstructed, including 13 with CHDs. The following CHDs were assessed: critical pulmonary stenosis (fig 1A), transposition of the great arteries (fig 1B), complete atrioventricular septal defect (fig 1C), hypoplastic left heart syndrome (fig 1D), left ventricular diverticulum (fig 1E), muscular interventricular communication (fig 1F), common arterial trunk, tetralogy of Fallot, Ebstein's anomaly, rhabdomyomas, left ventricular aneurysm, double outlet right ventricle with anterior aorta (Taussig-Bing), and tetralogy of Fallot with pulmonary valve agenesis. Fetal cardiac volumes were acquired using STIC during 3D fetal echocardiography at the Federal Universities of Rio de Janeiro and São Paulo. After storage on USB devices, heart segmentation (3D Slicer software) was performed using MeshLab 2023.12 (Pisa, Italy). The resulting models were then sent to the Biodesign Laboratory DASA at the Pontifical Catholic University of Rio de Janeiro (PUC-Rio) for 3D printing using MediJet J5 (MediJet 3D Printer, Stratasys, USA) (Video S1).

In summary, 3D physical models provide a spatial view of the fetal heart, allowing parents to better understand fetal heart malformations. They also enable interactive discussions among a multidisciplinary team, including maternal-fetal medicine specialists, obstetricians, neonatologists, pediatric cardiologists, and cardiovascular surgeons, to plan delivery, postnatal care, and cardiac surgery.

References

1. Hoffman JI, Kaplan S. The incidence of congenital heart disease. J Am Coll Cardiol 2002 19;39:1890-1900.
2. DeVore GR, Falkensammer P, Sklansky MS, Platt LD. Spatio-temporal image correlation (STIC): new technology for evaluation of the fetal heart. Ultrasound Obstet Gynecol 2003;22:380-387
3. Giffoni MC, Bravo-Valenzuela NJ, Araujo Júnior E, Ximenes RS, Werner H. Fetal Heart Rhabdomyomas: Three-dimensional Virtual Reconstruction Model. J Obstet Gynaecol Can 2025;47:103045.
4. Nieblas CO, Bravo-Valenzuela NJ, Araujo Júnior E, Werner H. Fetal transposition of the great arteries: 3D virtual and physical models from ultrasound datasets. Int J Cardiovasc Imaging 2024;40:1157-1158.
5. Oliveira Nieblas C, Araujo Júnior E, Bravo-Valenzuela NJM, Castro Giffoni M, Pereira Leite MF, Werner H. 3D ultrasound of fetal congenital heart disease: findings from virtual and physical models. J Ultrason 2025;25:20250026.
6. Werner H, Lopes J, Ribeiro G, Raposo AB, Trajano E, Araujo Júnior E. Three-dimensional virtual traveling navigation and three-dimensional printing models of a normal fetal heart using ultrasonography data. Prenat Diagn 2019;39:175-177.
7. Galliotto F, Veronese P, Cerutti A, et al. Enhancing parental understanding of congenital heart disease through personalized prenatal counseling with 3D printed hearts. Prenat Diagn 2024;44:725-732.

Supplementary material

Video S1. Three-dimensional printing of fetal heart physical models using the MediJet J5 (MediJet 3D Printer, Stratasys, USA).

Prenatal visualization of the fetal uterus

Zheng-feng Zhu

Ultrasound Department, Zhengzhou University Third Hospital and Henan Province and Children's Hospital, Zhengzhou, China

Received 30.12.2025 Accepted 28.01.2026
Med Ultrason
2026, Vol. 28, No 2, 242-243, DOI: 10.11152/mu-4621,
Corresponding author: Zheng-feng Zhu
ZhengZhou University Third Hospital and Henan Province Women and Children's Hospital, Zhengzhou, China
E-mail: tiansy728@163.com

To the Editor,

Ultrasonographic diagnosis of fetal uterus plays an important role in the evaluation of female fetal development. The sonographic technique concerning the fetal uterus exists is scarce. Soriano et al. [1] measured the uterus by a transverse axial scan at the fetal bladder level

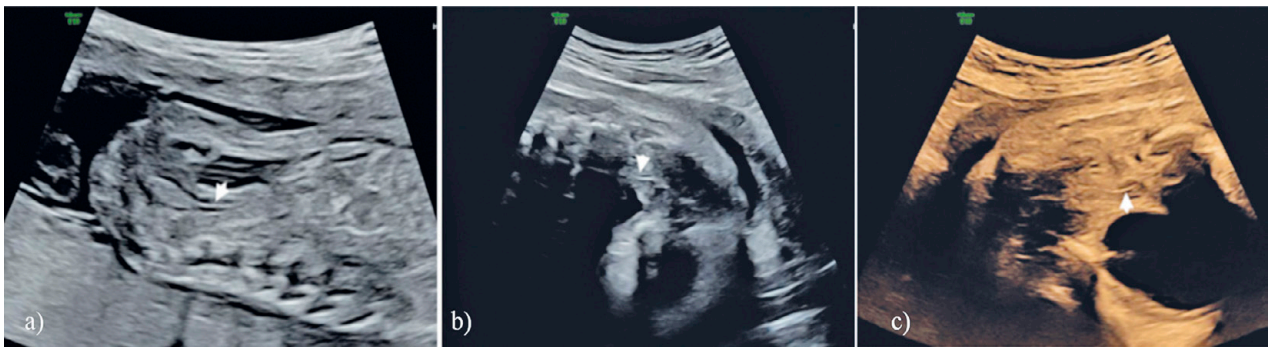


Fig 1. 2D ultrasound images of normal female fetuses at a) 23, b) 33, and c) 36 weeks of gestation. Note the endometrial line-like echo (arrows) behind the bladder.

transabdominal, and transvaginal in some case located deeply. Some publications referring to fetal sex assignment did not describe the sonographic appearance of fetal uterus [2,3]. Recently, Azumendi et al established a novel technique which carries relatively simple steps to identify the fetal cervix-uterus complex [4]. This technique simplified the assessment of the uterus into three steps: first, locate the fetal bladder and adjust the image in a suitable size and contrast; second, identify the vertebral body and rectum in the same view, then, the round structure between the bladder anteriorly and the bowel posteriorly is considered the uterus, as if the uterus is absent, the bowel and the bladder will be placed close to each other.

Here, we present our experience with normal prenatal cervix-uterus complex. When a round solid and heterogeneous structure between the bladder and the rectum is obtained in transverse view as Azumendi et al mentioned [4], we rotated the probe to obtain the sagittal view, under the premise that the bladder is full or half full. Then an endometrial line-like echo could be observed. Herein we presented three normal cases. The first case was at 23 weeks; case 2 was at 33 weeks; case 3 was at 36 weeks (fig 1). It can provide intuitive evidence for the identification of the cervix-uterus complex. The endometrial line also would help identify whether it is the uterus or the rectum, which can be superimposed on space theoretical basis that the space in males and females was different between the bladder and the rectum [2-4]. It could be achieved either in the spine anteriorly or posteriorly. It is accessible and has perspective for acquiring the endometrial line-like echoes.

Prenatal identification of internal organs is important to distinguish between normal fetuses and abnormalities. Prenatal visualization of fetal uterus with endometrial line-like echo maybe requires larger numbers to further refine the values.

References

1. Soriano D, Lipitz S, Seidman DS, et al. Development of the fetal uterus between 19 and 38 weeks of gestation: in-utero ultrasonographic measurements. Hum Reprod 1999;14:215-218.
2. Glanc P, Umranikar S, Koff D, et al. Fetal sex assignment by sonographic evaluation of the pelvic organs in the second and third trimesters of pregnancy. J Ultrasound Med 2007;26:563-569.
3. Aydin E, Holt R, Chaplin D, et al. Fetal anogenital distance using ultrasound. Prenat Diagn 2019;39:527-535.
4. Azumendi P, Borenstein M, Jiménez JS, et al. Prenatal visualization of the fetal uterus in routine 2D ultrasound examination. Ann Med 2025;57:2449226.

Ultrasound diagnosis of median nerve compression associated with an arterial variant at the elbow

Wei-Ting Wu[1,2], Ke-Vin Chang[1,2,3], Levent Özçakar[4]

[1]Department of Physical Medicine and Rehabilitation and Community and Geriatric Research Center, National Taiwan University Hospital, Bei-Hu Branch, [2]Department of Physical Medicine and Rehabilitation, National Taiwan University College of Medicine, Taipei, Taiwan, [3]Center for Regional Anesthesia and Pain Medicine, Wang-Fang Hospital, Taipei Medical University, Taipei, Taiwan, [4]Department of Physical and Rehabilitation Medicine, Hacettepe University Medical School, Ankara, Turkey

To the Editor,

A 54 year-old male presented with intermittent numbness along the radial two-thirds of the palm (corresponding to the median nerve distribution) aggravated by elbow flexion and forearm rotation. There was no history of acute trauma, and electrodiagnostic testing yielded inconclusive findings. Physical examination revealed a positive Tinel sign over the elbow. Ultrasound examination of the elbow was performed to assess possible nerve compression.

Initially, the transducer was placed over the antecubital fossa in the short-axis to evaluate the morphology of the median nerve. In contrast to the normal median nerve adjacent to a single brachial artery (fig 1a), it was accompanied by two hypoechoic tubular structures on the affected side (fig 1b). As the transducer was advanced distally, the median nerve was observed to be compressed between two tubular structures (fig 1c,d). Spectral Doppler demonstrated arterial flow within those hypoechoic structures (fig 1e). As such, the variant (brachioradial) artery was identified causing median nerve compression at the elbow (fig 1f).

Median nerve entrapment at the elbow is uncommon and frequently underdiagnosed because its clinical presentation often overlaps with distal median neuropathies. Beyond muscular and fibrous causes [1] e.g. pronator teres, sublimus bridge of the flexor digitorum superficialis, and anterior interosseous nerve syndromes, arterial anatomical variations within the cubital fossa represent a distinct but underrecognized mechanism of median nerve compression. Anatomical studies have demonstrated that arterial variants, such as superficial brachial or brachioradial artery, may course superficial or anterior to the me-

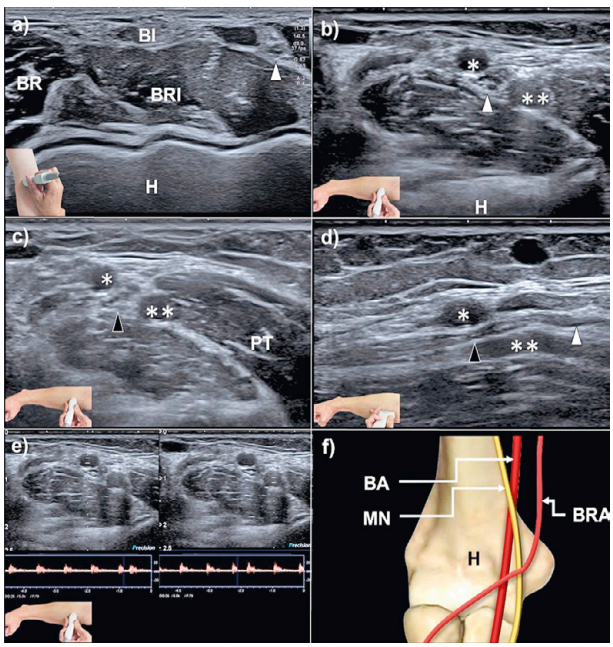


Fig 1. Ultrasonography (short-axis view) of the normal median nerve at the antecubital fossa (a). On the symptomatic side, the median nerve is accompanied by two hypoechoic structures (b) and appears flattened/entrapped on both short- (c) and long-axis (d) views. Spectral Doppler imaging confirms arterial flow within both hypoechoic structures (e), consistent with the corresponding anatomical illustration (f). Asterisk: brachial artery; double asterisk: brachioradial artery; white arrowhead: median nerve; black arrowheads: entrapment site; H: humerus; PT: pronator teres; BA: brachial artery; BRA: brachioradial artery; MN: median nerve; BRI: brachialis; BR: brachioradialis.

Received 30.12.2025 Accepted 01.03.2026
Med Ultrason
2026, Vol. 28, No 2, 244-245, DOI: 10.11152/mu-4622,
Corresponding author: Ke-Vin Chang, MD, PhD
Department of
Physical Medicine and Rehabilitation,
National Taiwan University Hospital,
Bei-Hu Branch and
National Taiwan University College
of Medicine,
Taipei, Taiwan
E-mail: kvchang011@gmail.com

dian nerve [2]. In rare configurations, hypoplastic arterial segments or prominent cubital anastomoses may cross or tether the nerve, creating a potential site of neurovascular conflict [3].

High-resolution ultrasound enables translation of detailed anatomical observations into accurate diagnoses [4]. Doppler imaging further enhances diagnostic confidence by demonstrating arterial pulsatility. Precise identification of vascular variants may prevent misdiagnosis as distal nerve entrapment or cervical pathology and facilitates management. These findings underscore the importance of extending ultrasound evaluation in patients with unexplained median nerve symptoms. Not to mention, recognition of such arterial variants is essential during invasive procedures to minimize the risk of iatrogenic injury.

References

1. Chang K-V, Wu W-T, Hsu P-C, Yang Y-C, Özçakar L. Ultrasonography in pronator teres syndrome: Dynamic examination and guided hydrodissection. Pain Medicine 2022;23:219-220.
2. Glin M, Zielinska N, Ruzik K, Karauda P, Konschake M, Olewnik L. Morphological variations of the brachial artery and their clinical significance: a systematic review. Surg Radiol Anat 2023;45:1125-1134.
3. Haladaj R, Wysiadecki G, Polguj M, Topol M. Hypoplastic superficial brachioradial artery coexisting with atypical formation of the median and musculocutaneous nerves: a rare combination of unusual topographical relationships. Surg Radiol Anat 2019;41:441-446.
4. Wu W-T, Chang K-V, Hsu Y-C, et al. Ultrasound imaging and guidance for distal peripheral nerve pathologies at the wrist/hand. Diagnostics 2023;13:1928.

"Selfie elbow": smartphone-savvy ultrasound examination

Ahmad Jasem Abdulsalam[1], Vincenzo Ricci[2], Levent Özçakar[3]

[1]Department of Physical Medicine and Rehabilitation, Mubarak Alkabeer Hospital, Jabriya Kuwait, [2]Physical and Rehabilitation Medicine Unit, Luigi Sacco University Hospital, Aziende Socio Sanitarie Territoriale Fatebenefratelli Sacco, Milan, Italy, [3]Department of Physical and Rehabilitation Medicine, Hacettepe University Medical School, Ankara, Turkey

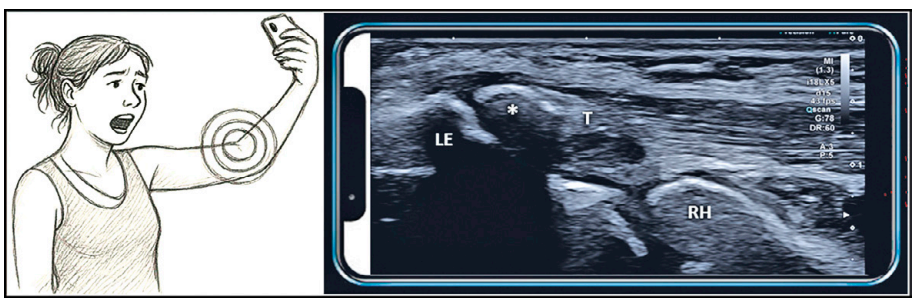


Fig 1. Metaphoric drawing and 'sonographic selfie' showing calcification (white asterisks) of the common extensor tendon (T) due to chronic mechanical overload while keeping the smartphone stable during several daily shots. RH: radial head, LE: lateral epicondyle

To the Editor,

The digital revolution has quietly infiltrated our musculoskeletal clinics. Millions of smartphone users are developing lateral elbow pain from prolonged selfie photography and texting postures. Accordingly, it is high time to ask how routine technology-induced biomechanical stress is addressed during physiatry/ultrasound (US) examination.

The clinical picture is deceptively familiar i.e. lateral epicondylar tenderness and/or pain with resisted wrist extension, commonly known as "tennis elbow" (fig 1). However, smartphone-related elbow pain may present with subtle differences that warrant closer US scrutiny. Using high-frequency transducers, dynamic assessment

Received 09.02.2026 Accepted 01.03.2026
Med Ultrason
2026, Vol. 28, No 2, 245-246, DOI: 10.11152/mu-4623,

Corresponding author: Ahmad Jasem Abdulsalam
Mubarak Al-Kabeer Hospital,
Jabriya, Kuwait
E-mail: dr.ahmad.j.abdulsalam@gmail.com

during simulated smartphone positioning can effectively be performed – in addition to systematic entheseal imaging for common extensor tendon origin (e.g. tendon hypoechogenicity/thickening, cortical irregularity) (Video 1 and 2, on the journal site) [1-3]. Further, given the prolonged forearm rotation inherent in selfie photography, the posterior interosseous nerve also deserves particular attention as it traverses the supinator muscle. While established nerve entrapment criteria apply, the repetitive nature of smartphone use may cause subtle morphological changes that static imaging overlooks [3].

Not to mention (from a practical standpoint), in case an intervention is planned/needed, US guidance is again contributory for procedure precision as well as clinical decision making before and close follow up thereafter. In short, our 'routine' elbow US examinations need to encompass also additional dynamic scans in accordance with our patients' evolving lifestyles – currently related to smartphones but who knows in the future what's next?

References

1. Levin D, Nazarian LN, Miller TT, et al. Lateral epicondylitis of the elbow: US findings. Radiology 2005;237:230-234.
2. Mezian K, Sobotová K, Angerová Y. Sonographic elbow scanning is not yoga exercise. Adv Rheumatol 2019;59:33.
3. Ricci V, Cocco G, Mezian K, et al. Anatomy and sonographic examination for lateral epicondylitis: EUROMUSCULUS/USPRM Approach. Am J Phys Med Rehabil 2023;102:300-307.

Video legends

Video 1. Hypoechoic thickening of the common extensor tendon at the lateral epicondyle with intra-tendinous hyperemia due to insertional tendinosis.
Video 2. Avulsion of the deep fibers of the common extensor tendon from the lateral epicondyle. The proximal stump is visible between the superficial fibers of the tendon and the radial collateral ligament.

Intramyometrial cyst mimicking ovarian endometriotic cyst

Shiyun Peng

Department of Ultrasound West China Second University Hospital Sichuan University, Sichuan, China

To the Editor,

A 39-year-old female visited our clinic with lower abdominal pain for over one month. She had a history of adnexa mass for about 3 years.

A transvaginal ultrasound scan showed a large, well-defined, anechogenic, round cystic mass measuring 8.9x5.7x6.0 cm with some septations and internal floating echogenicities at the right adnexa area (fig 1ab), while both ovaries present normal with clear boundaries and the mass located close to uterus. The laboratory findings, including the biochemical and tumor markers (carcinoembryonic antigen, carbohydrate antigen 125), were within the normal ranges.

The patient underwent laparoscopic surgery for adnexa mass which was found to be located on the right anterior uterine wall, with soft texture and intact capsule, smooth walls and clear fluid inside (fig 1c). Postoperative pathology showed that the mass was an intramyometrial cyst with adenomyosis (fig 1d).

Intramyometrial cysts are rare benign conditions. Cystic masses of the uterus are mainly classified into two groups: congenital and acquired. Congenital cysts include Wolffian duct (mesonephric) cysts and Müllerian (paramesonephric) duct cysts, and acquired cysts include adenomyosis, cervical nabothian cysts, cystic degeneration of intrauterine fibroid, cystic adenomatoid tumor, adenocystic tumor, intramyometrial hydrosalpinges and parasitic cysts such as echinococcal cyst [1-7]. Age and parity were significantly lower in patients with non-fibroid cysts, and non-fibroid cysts are more likely to be diagnosed as adnexal enlargements [8].

Received 08.01.2026 Accepted 01.03.2026
Med Ultrason
2026, Vol. 28, No 2, 246-247, DOI: 10.11152/mu-4624,
Corresponding author: Shiyun Peng
Department of Ultrasound West China
Second University Hospital
Sichuan University,
1416 Chenglong Ave,
Chengdu, Sichuan,
China 610066
E-mail: raphia@yeah.net

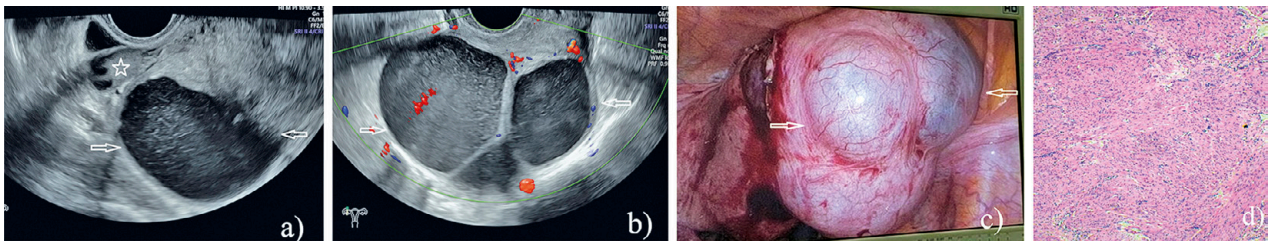


Fig 1. a) Gray scale ultrasound showed the cyst (arrow) with a clear boundary from the right ovary (star); b) Color-doppler ultrasound of the cyst with septations (arrow); c) Laparoscopic image of the cyst (arrow); d) HE staining of the cyst.

In conclusion, in patients with pelvic cystic mass, when both ovaries present normal and the mass is located close to the uterus, intramyometrial cysts should be considered as a possible diagnosis.

References

1. Sherrick JC, Vega JG. Congenital intramural cysts of the uterus. Obstet Gynecol 1962;19:486–493.
2. Chongchitnant N, Otken LB Jr. Intrauterine hydrosalpinx. Hum Pathol 1984;15:592–594.
3. Sosnovski V, Barenboim R, Cohen HI, Bornstein J. Complex Nabothian cysts: A diagnostic dilemma. Arch Gynecol Obstet 2009;279:759–761.
4. Kim JY, Jung KJ, Sung NK, Chung DS, Kim OD, Park S. Cystic adenomatoid tumor of the uterus. AJR Am J Roentgenol 2002;179:1068–1070.
5. Bais A, Shirodkar SD, Nayak A, Jashnani K. A case of rare Mullerian anomaly– Functional rudimentary uterine horn. Bombay Hosp J 2008;50:116–118.
6. Jung WY, Shin BK, Kim I. Uterine adenomyoma with uterus like features: A case report of two cases. Int J Surg Pathol 2002;10:163–166.
7. Gershon CE, Omer AZ, Mariam S, Hartmut EB. Giant adenomyotic cyst of the uterus. Br J Obstet Gynecol 1993;100:596–598.
8. Protopapas A, Milingos S, Markaki S, et al. Cystic uterine tumors. Gynecol Obstet Invest 2008;65:275-280.

Pouch-like infective endocarditis of the mitral valve

Yuanyuan Cui[1], Xuejie Li[2]

[1]Department of Anesthesiology, Shenzhen People's Hospital, The First Affiliated Hospital, Southern University of Science and Technology, The Second Clinical Medical College, Jinan University, Shenzhen, [2]Department of Anesthesiology, West China Hospital, Sichuan University and The Research Units of West China, Chinese Academy of Medical Sciences, Chengdu, China

To the Editor,

We report the case of a 56-year-old male patient admitted with dyspnea and fever and was diagnosed with infective endocarditis (IE) in the local hospital. The prescription was adjusted to piperacillin sodium and tazobactam combined with amikacin. The temperature eventually normalized, and the blood culture was negative six days later. He was transferred to our center for mitral valve repair.

Intraoperative transesophageal echocardiography (TEE) examination revealed severe mitral regurgitation, posterior mitral valve prolapse into the left atrium combined with pouch-like changes (fig 1a,b). The patient underwent mitral mechanical valve replacement through median thoracotomy under cardiopulmonary bypass. Intraoperative exploration revealed that the mitral valve leaflet infective endocarditis manifests with pouch-like structures (fig 1c). Mitral repair could not be performed due to the severity of the mitral valve lesion. The patient underwent mechanical mitral valve replacement without

Received 29.01.2026 Accepted 01.03.2026
Med Ultrason
2026, Vol. 28, No 2, 247-248, DOI: 10.11152/mu-4625,
Corresponding author: Xuejie Li
Department of Anesthesiology, West China Hospital, Sichuan University and The Research Units of West China (2018RU012), Chinese Academy of Medical Sciences, Chengdu 610041, Sichuan Province, China
E-mail: lizuima@hotmail.com

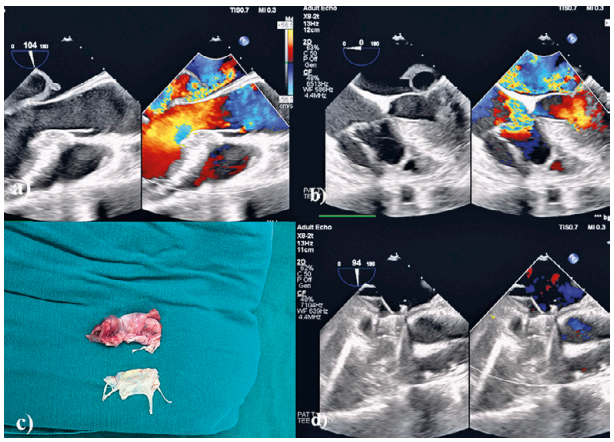


Fig 1. a) The mid-esophageal long-axis view revealed severe mitral regurgitation, posterior mitral valve prolapse into the left atrium, and combined with pouch-like changes; b) The mid-esophageal long-axis view also revealed a pouch-like mitral posterior valve; c) Intraoperative exploration revealed that the mitral valve leaflet infective endocarditis manifests with pouch-like structures; d) The patient underwent mechanical mitral valve replacement without paravalvular leakage.

paravalvular leakage (fig 1d) and was discharged uneventfully 12 days postoperatively.

Native valve IE is uncommon, with an incidence of approximately 2 to 10 cases per 100,000 person-years. Worldwide, gram-positive bacteria account for approximately 80% of cases of native-valve infective endocarditis [1]. The presumed initiating event is injury to the valvular endothelium or endocardium. Mitral repair should be favored over replacement in IE when there is no evidence of local extension of the infections and if valve leaflets have not degenerated [2]. Unfortunately, mitral repair couldn't be performed in the patient due to the severe mitral valve lesion. In general, IE involves both the mitral anterior and posterior valves. We report a rare case of IE involving the mitral posterior valve alone and presenting a pouch-like structure.

References

1. Chambers HF, Bayer AS. Native-Valve Infective Endocarditis. N Engl J Med 2020;383:567-576.
2. Comentale G, Ahmadi-Hadad A, Moldon HJ, et al. Comparative Outcomes of Mitral Valve Repair Versus Replacement in Infective Endocarditis: A 16-Year Meta-Analysis of Time-to-Event Data From Over 4000 Patients. Am J Cardiol 2025;246:33-42.

Sonographic features of low-grade appendiceal mucinous neoplasms

Hongran Pan, Haotian Zhao, Yi Liu, Caina Xu, Li Li

Department of Ultrasound, Hebei General Hospital, Shijiazhuang, Hebei, China

To the Editor,

A 75-year-old female was scheduled for varicose vein surgery. During a routine preoperative venous vascular ultrasound examination in the department of ultrasound, a mixed-echo mass was incidentally detected in the right lower abdomen. The mass was situated anterior to the right iliac vessels, adjacent to the appendix. The mass measured approximately 50.7×29.9×28.3 mm, with relatively well-defined borders and heterogeneous internal echogenicity (fig 1a). Color Doppler ultrasonography demonstrated the absence of significant blood flow signals within the lesion (fig 1b). She underwent computed tomography (CT), which revealed marked appendiceal thickening with wall enhancement, intraluminal calcification, and hypodense filling of the lumen (fig 1c). Review of the patient's medical records revealed that the pathological diagnosis was a low-grade appendiceal mucinous neoplasm (LAMN) (fig 1d).

Appendiceal neoplasms are relatively uncommon findings in appendectomy [1]. Among these, LAMN is a distinct entity. It is reported that approximately 26% of patients with LAMN who undergo appendectomy experience recurrence or mortality [2]. Histologically, in addition to low-grade cytological atypia, LAMN is characterized by several architectural features: obliteration of

Received 05.03.2026 Accepted 08.05.2026
Med Ultrason
2026, Vol. 28, No 2, 248-249, DOI: 10.11152/mu-4626,
Corresponding author: Li Li
Department of Ultrasound, Hebei General Hospital, 348 Heping West Road, Shijiazhuang, Hebei, China
E-mail: shrmgnk@126.com

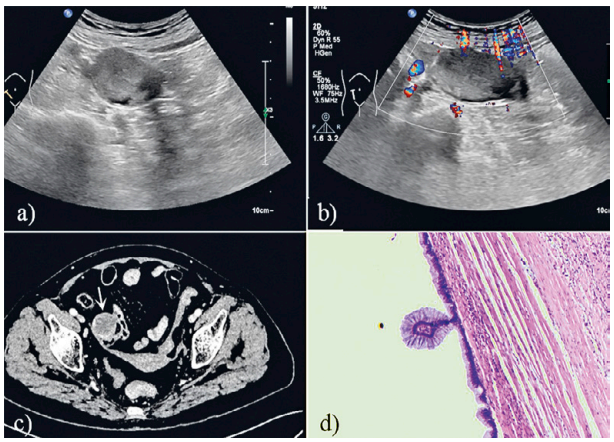


Fig 1. a) Ultrasonography identified a heterogeneous mass in the right lower quadrant; b) Color Doppler showed no obvious blood flow signal inside the mass; c) Computed tomography (CT) showed significant appendiceal wall thickening and calcification, accompanied by low-attenuation intraluminal content (white arrow); d) The histopathological features were consistent with a diagnosis of low-grade appendiceal mucinous neoplasm (LAMN).

the muscularis mucosae, submucosal fibrosis, "pushing" invasion (manifesting as expansive or diverticulum-like growth), dissection of acellular mucin within the wall, a villous or flat epithelial growth pattern, appendiceal or mucin rupture, and the presence of LAMN cells beyond the appendix [3]. On ultrasonography, LAMN is most characteristically manifested as a cystic dilatation of the appendix. The appendix is markedly enlarged (diameter often >1.5 cm), presenting as a tubular or ovoid, anechoic to hypoechoic structure. The wall may be either thinned or thickened. The presence of mural calcifications is a notable sign. The internal content typically demonstrates homogeneous, low-level echoes and an absence of flow on color Doppler examination.

In the treatment of LAMN, surgical resection is currently the preferred option. Early detection and treatment of LAMN are crucial for reducing the risk of pseudomyxoma peritonei and improving patients' prognosis. As a non-invasive examination method, ultrasound holds significant value in the screening and diagnosis of LAMN.

References

1. Sueda T, Murata K, Takeda T, et al. Survival outcomes of appendiceal mucinous neoplasms by histological type and stage: Analysis of 266 cases in a multicenter collaborative retrospective clinical study. Ann Gastroenterol Surg 2019;3:291-300.
2. Fournier K, Rafeeq S, Taggart M, et al. Low-grade Appendiceal Mucinous Neoplasm of Uncertain Malignant Potential (LAMN-UMP): Prognostic Factors and Implications for Treatment and Follow-up. Ann Surg Oncol 2017;24:187-193.
3. Carr NJ, Cecil TD, Mohamed F, et al. A consensus for classification and pathologic reporting of pseudomyxoma peritonei and associated appendiceal neoplasia: the results of the peritoneal surface oncology group international (PSOGI) modified Delphi process. Am J Surg Pathol 2016; 40:14-26.

Prenatal sonographic diagnosis of oculo-auriculo-vertebral spectrum in a mid-trimester fetus

Jing Wang, Hong Luo

Department of Ultrasound, West China Second Hospital of Sichuan University, Key Laboratory of Birth Defects and Related Diseases of Women and Children (Sichuan University), Ministry of Education, Chengdu, Sichuan, China

Received 02.03.2026 Accepted 08.05.2026
Med Ultrason
2026, Vol. 28, No 2, 249-250, DOI: 10.11152/mu-4627,
Corresponding author: Hong Luo
Department of Ultrasound, West China Second University Hospital, Sichuan University, 20 South Renmin Road, Chengdu 610041, China
Email: hxeycsklh@163.com

To the Editor,

A 29-year-old primigravid woman was referred to our center at 23 weeks' gestation due to the suspicion of congenital heart disease. Examination of the fetal head revealed fetal micrognathia (fig 1a) with the inferior facial angle (IFA) of 44°and mild left-sided facial cleft (Tessier cleft no. 7, fig 1d). A redundant tag was detected in both

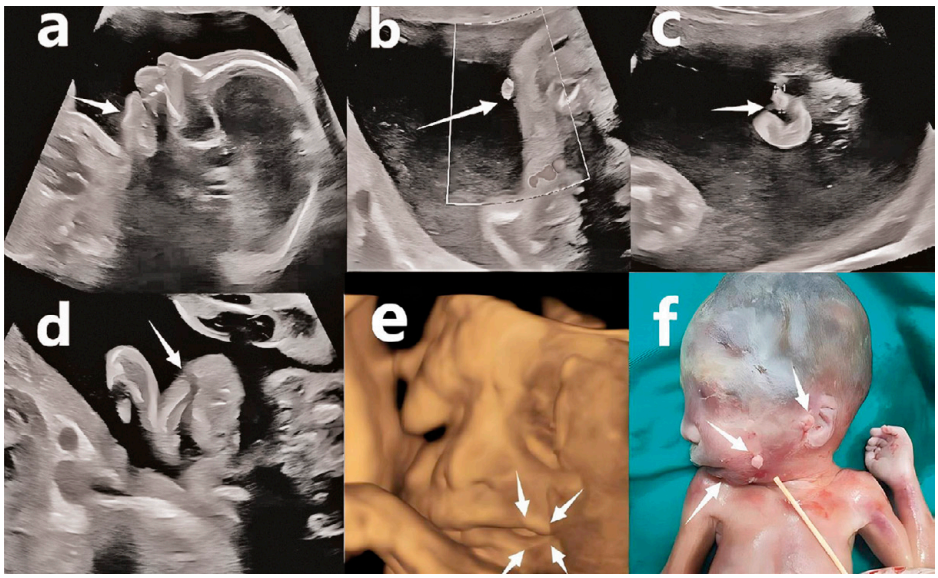


Fig 1. Prenatal multimodal ultrasound and postnatal manifestation of a OAVS fetus: a) Two-dimensional grayscale ultrasound showed micrognathia in the mid-sagittal facial view; b) Color Doppler ultrasound in the coronal view of the fetal face revealed a facial tap; c) and d) Grayscale ultrasound showed a preauricular tap in left ear and a facial cleft; e) Three-dimensional ultrasound imaging revealed a facial cleft in the fetus; f) Gross specimen showed a left facial and preauricular tap, micrognathia, and a left facial cleft.

the left facial and preauricular area (fig 1b,c). A more significant image of left-side facial cleft was observed by 3-dimensional ultrasound (fig 1e). The fetal echocardiography revealed a smaller left atrium lacking a clear connection to the pulmonary veins, which formed a common trunk via a vertical vein (2.4 mm). Additional findings included a ventricular septal defect (VSD) of 3 mm in the upper septum and a hypoplastic transverse aortic arch. The diagnosis of oculo-auriculo-vertebral spectrum **(**OAVS) was considered. The patient decided to terminate the pregnancy. The stillborn foetus was found with significantly retrognathic mandible, a left-side cleft about 0.5 cm, a left preauricular tag and a left facial tag (fig 1f). The final diagnosis of OAVS was therefore confirmed.

OAVS is a congenital disorder originating from developmental anomalies of the first and second branchial arches. Its incidence is estimated to be one in 3000 to 5000 [1,2]. Most cases are sporadic, with no clear family genetic history and a low recurrence risk [3]. For facial deformities, the first detected abnormalities were skin tags on the face and preauricular area. When scanning the upper lip, it is crucial to fully display the bilateral labial commissures, otherwise, there is a risk of missing a diagnosis of mild facial clefts. In accordance with the minimum diagnostic criteria of OAVS, if facial or preauricular skin tags are observed, thorough examination of structures affected by the first and second branchial arches should be conducted.

This case reinforces the value of prenatal ultrasound in identifying OAVS, especially when multiple suggestive features coexist. Sonographers' familiarity with the OAVS spectrum is vital for timely diagnosis.

Acknowledgment: This research was supported by the Program of Science and Technology Department of Sichuan Province (2025ZNSFSC0345)

References

1. Chen H, Shen W. Goldenhar Syndrome Complicated by Hemifacial Microsomia and Unilateral Cleft Palate Absence. J Craniofac Surg 2024, doi: 10.1097/SCS.0000000000010555.
2. Benacerraf BR, Frigoletto FD, Jr. Prenatal ultrasonographic recognition of Goldenhar's syndrome. Am J Obstet Gynecol 1988;159:950-952.
3. Estandia-Ortega B, Fernández-Hernández L, Alcántara-Ortigoza MA, et al. Proposed clinical approach and imaging studies in families with oculo-auriculo-vertebral spectrum to assess variable expressivity. Am J Med Genet A 2022; 188:1515-1525.

Inflammatory nodule after hyaluronic acid and hyaluronidase injection at ultra-high-frequency ultrasound

Corrado Tagliati[1], Claudio Ventura[2], Marco Fogante[2], Giulio Rizzetto[3], Edoardo De Simoni[3], Matteo Candelora[3], Marco Matteucci[3], Sara Belleggia[3], Giulio Argalia[2], Elisa Molinelli[3], Annamaria Offidani[3], Oriana Simonetti[3]

[1]AST Ancona, Ospedale di Comunità Maria Montessori di Chiaravalle, Chiaravalle, [2]Maternal-Child, Senological, Cardiological Radiology and Outpatient Ultrasound, Department of Radiological Sciences, University Hospital of Marche, Ancona, [3]Department of Clinical and Molecular Sciences, Dermatology Clinic, Polytechnic Marche University, Ancona, Italy

To the Editor,

Here, we present a case of a 40-year-old female patient who performed cheek hyaluronic acid injection. After few weeks, a palpable nodule was detected and hyaluronidase was injected. Subsequently, ultra-high-frequency ultrasound (70 MHz probe) examination of a palpable nodule at right cheek was performed and showed an iso-hypoechoic hyper-vascular lesion with peripheral and internal vascularization at Doppler ultrasound. It was 3 mm thick and its maximum transverse diameter was 7 mm. Ultrasound usefulness in evaluating filler materials, guiding injection and assessing complications were reported in previously published articles [1-11]. However, to the best of our knowledge, this is the first case of inflammatory nodule after hyaluronic acid and hyaluronidase injection at ultra-high-frequency ultrasound.

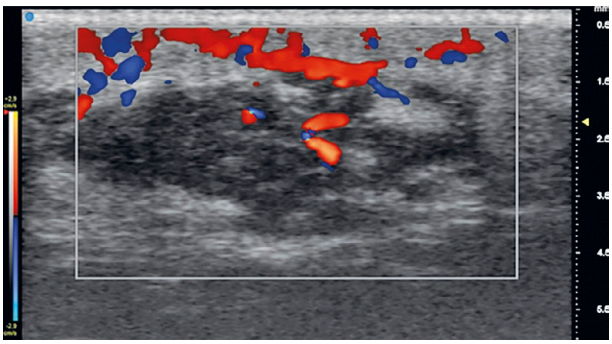


Fig 1. Ultra-high-frequency ultrasound (70 MHz probe) of a palpable iso-hypoechoic nodule at right cheek, with peripheral and internal vascularization

References

1. Wortsman X. Top applications of dermatologic ultrasonography that can modify management. Ultrasonography 2023;42:183-202.
2. Argalia G, Reginelli A, Molinelli E, et al. High-Frequency and Ultra-High-Frequency Ultrasound in Dermatologic Diseases and Aesthetic Medicine. Medicina (Kaunas) 2025;61:220.
3. Cavallieri FA, Balassiano LKA, Munhoz G, Tembra MF, Wortsman X. Ultrasound in Aesthetics: Filler and Non-Filler Applications. Semin Ultrasound CT MR 2024;45:251-263.
4. Fogante M, Carbon N, Argalia G. Clinical application of ultra-high frequency ultrasound: Discovering a new imaging frontier. J Clin Ultrasound 2022;50:817-825.
5. Chammas MC, Sigrist R, Alfageme F, et al.. WFUMB Position Paper: Consensus on Best Practice in Aesthetic Dermatologic Ultrasound. Ultrasound Med Biol 2025;51:2173-2193.
6. Vasconcelos-Berg R, Desyatnikova S, Bonavia P, Navarini A, Chammas MC. Sigrist R. Best Practices for the Use of High-Frequency Ultrasound to Guide Esthetic Filler Injections-Part 3: Lower Third of the Face. Diagnostics (Basel) 2025;15:921
7. Wortsman X, Valderrama Y, Ortiz-Orellana G, et al. International Multicentric Study on Ultrasound Characteristics, Layer Location, and Corporal Distribution of Granulomas After Cosmetic Fillers Injections. J Ultrasound Med 2025;44:1447-1455.
8. Vasconcelos-Berg R, Desyatnikova S, Bonavia P, Chammas MC, Navarini A, Sigrist R. Best Practices for the Use of High-Frequency Ultrasound to Guide Aesthetic Filler Injections-Part 2: Middle Third of the Face, Nose, and Tear Troughs. Diagnostics (Basel) 2024;14:2544.
9. Sigrist R, Fassina M, Wortsman X. Ultrasonographic Pattern of a New Generation of Polymethylmethacrylate at

Received 30.01.2026 Accepted 01.03.2026
Med Ultrason
2026, Vol. 28, No 2, 251-252, DOI: 10.11152/mu-4628,
Corresponding author: Corrado Tagliati
Via Lambro 5, 60126 Ancona,
Italy
E-amil: corrado.tagliati@gmail.com

High-Frequency and Ultra-High Frequency. Dermatol Surg 2025;51:226-228.
10. Sigrist R, Desyatnikova S, Chammas MC, Vasconcelos-Berg,R. Best Practices for the Use of High-Frequency Ultrasound to Guide Aesthetic Filler Injections-Part 1: Upper Third of the Face. Diagnostics (Basel) 2024;14: 1718.
11. Sigrist R, Noronha G, Quezada N, Wortsman X. Ultrasonographic Pattern of Poly- l -Lactic Acid at High-Frequency and Ultrahigh-Frequency. Dermatol Surg 2024;50:783-785.

Unlocking the scar: ultrasound-guided hydrodissection for post-surgical radial nerve entrapment following clinical plateau

Alan Chang[1], Shu-Mei Yang [1,2], Huey-Wen Liang[2], Chueh-Hung Wu[1,2]

[1]Department of Physical Medicine and Rehabilitation, National Taiwan University Hospital Hsin-Chu Branch, Hsinchu, [2]Department of Physical Medicine and Rehabilitation, National Taiwan University Hospital, College of Medicine, Taipei, Taiwan

To the Editor,

A 39-year-old male presented with persistent right wrist drop and radial sensory deficits 10 weeks post-open reduction and internal fixation for a humeral shaft fracture. Despite two months of conservative therapy, he remained at a clinical plateau (Medical Research Council [MRC] grade 0 of wrist extension with preserved elbow extension; absent compound muscle action potentials and sensory nerve action potentials in nerve conduction studies). Ultrasonography revealed a markedly edematous, hypoechoic radial nerve entrapped within dense postoperative scar tissue from the distal spiral groove to the elbow; anatomical continuity was preserved (fig 1a-c, Video S1 at the journal site).

Ultrasound-guided hydrodissection (HD) was performed using 5 mL of 5% dextrose (D5W) (Fig 1d, Video S2 at the journal site). Significant mechanical resistance was encountered initially, representing dense perineural adhesions. By 14 weeks post-injury (4 weeks after the initial HD session), electromyography demonstrated the first evidence of regenerative activity in the brachioradialis. Sensory symptoms nearly resolved after four sessions, while motor recovery followed a strict proximal-to-distal pattern. After 12 HD sessions, the patient achieved near-full motor recovery (MRC 5 wrist, 4+ finger extension) at 9.5 months. Notably, injection resistance decreased progressively across sessions, suggesting gradual nerve liberation from fibrotic tissue.

This case highlights HD as a therapeutic bridge during the 3-to-6-month window before considering surgical re-exploration. We propose that scar tissue acted as a rate-limiting factor in this case; HD successfully "unlocked" the nerve from the scar and was effective even after a 10-week clinical stagnation while initial recovery typically begins within 7–9 weeks [1]. Moreover, motor recovery may require a more intensive regimen than sensory alleviation [2]. This likely stems from the larger diameter and higher metabolic demands of motor fibers, which entail greater reinnervation complexity.

In conclusion, ultrasound-guided HD can facilitate recovery in post-surgical nerve entrapment even after a 10-week clinical plateau. While motor reinnervation may require more frequent intervention, the progressive reduction in injection resistance suggests that HD also serves as a valuable serial diagnostic tool for monitoring the resolution of perineural fibrosis.

Received 20.04.2026 Accepted 08.05.2026
Med Ultrason
2026, Vol. 28, No 2, 252-253, DOI: 10.11152/mu-4629,
Corresponding author: Chueh-Hung Wu, MD, PhD
Department of Physical Medicine and Rehabilitation,
National Taiwan University Hospital
No.1, Changde St, Taipei,
Taiwan
E-mail: nojred@gmail.com;
b88401062@ntu.edu.tw

References

1. Shao YC, Harwood P, Grotz MR, Limb D, Giannoudis PV. Radial nerve palsy associated with fractures of the shaft

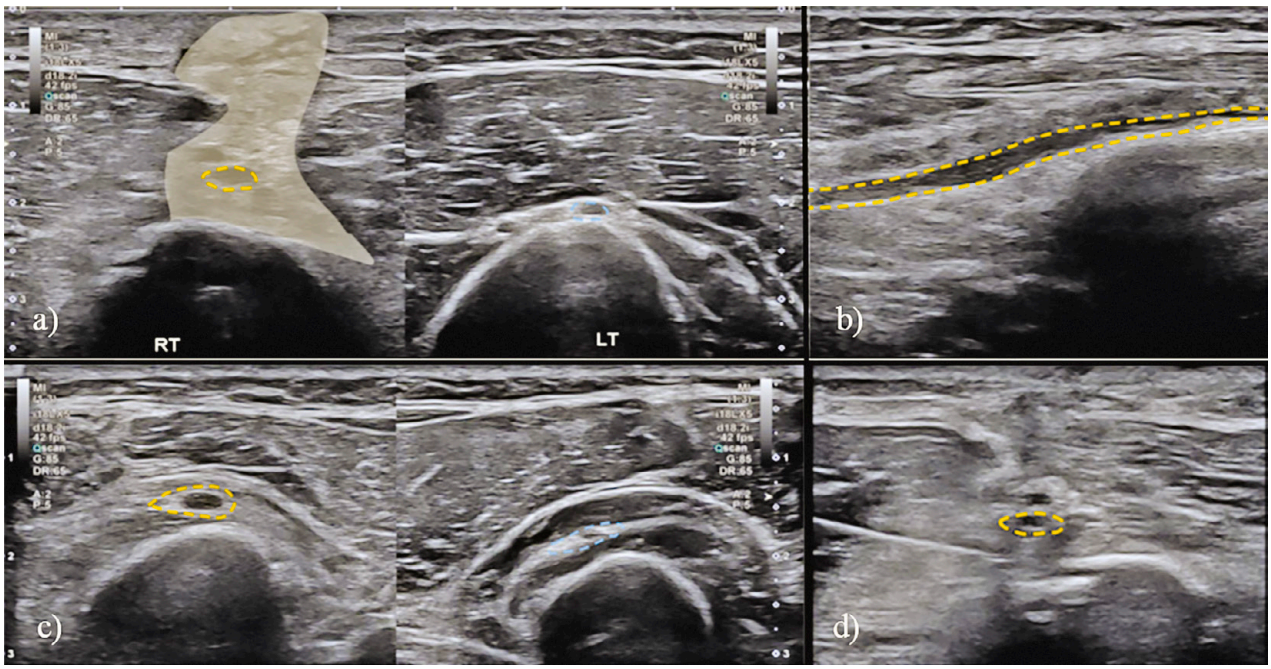


Fig 1. Ultrasonography of the radial nerve: a) Transverse view showed edematous radial nerve (yellow circle) within scar (shaded area), right (RT) comparing with left (LT); b) Longitudinal view showed preserved continuity of the radial nerve (yellow dashed line); c) Swollen deep branch at the supinator level (yellow circle) (right comparing with left); d) Hydrodissection procedure liberating the nerve.

of the humerus: a systematic review. J Bone Joint Surg Br 2005;87:1647-1652

2. Wu CH, Boudier-Revéret M. Ultrasound-Guided Steroid Injections for Lateral Antebrachial Cutaneous Nerve Entrapment Within Postsurgical Scar. Am J Phys Med Rehabil 2019;98:e106.

Supplementary material

Video S1. Transverse view showing radial nerve entrapment at the distal spiral groove level. Video S2. Ultrasound-guided hydrodissection of the radial nerve using 5% dextrose.